Received: 20 December 2019 | Accepted: 28 September 2020
DOI: 10.1002/hyp.13925

USING WATER AGE TO EXPLORE HYDROLOGICAL PROCESSES IN CONTRASTING ENVIRONMENTS

WILEY

Modelling non-stationary water ages in a tropical rainforest: A preliminary spatially distributed assessment

Alicia Correa[1,6] | Christian Birkel[1,2] | Jason Gutierrez[1] | Joni Dehaspe[1,3] | Ana María Durán-Quesada[4] | Chris Soulsby[2] | Ricardo Sánchez-Murillo[5]

[1]Department of Geography and Water and Global Change Observatory, University of Costa Rica, San José, Costa Rica
[2]Northern Rivers Institute, University of Aberdeen, Aberdeen, Scotland
[3]Umweltforschungszentrum Leipzig, Leipzig, Germany
[4]Atmospheric, Oceanic and Planetary Physics Department; Climate System Observation Laboratory School of Physics and Geophysical Research Center (CIGEFI), University of Costa Rica, San José, Costa Rica
[5]Stable Isotopes Research Group and Water Resources Management Laboratory, Universidad Nacional, Heredia, Costa Rica
[6]Centre for International Development and Environmental Research (ZEU), Justus Liebig University, Giessen, Germany

Correspondence
Alicia Correa, Department of Geography and Water and Global Change Observatory, University of Costa Rica, San José, Costa Rica.
Email: alicia.correa@ucr.ac.cr

Funding information
Leverhulme Trust; IsoNet and the University Centre for Advanced Studies, Grant/Award Number: B8276; Ministry of Science and Technology of Costa Rica (MiCITT), Grant/Award Number: B7507; University of Costa Rica, Grant/Award Number: B8709

Abstract

Pristine tropical forests play a critical role in regional and global climate systems. For a better understanding of the eco-hydrology of tropical "evergreen" vegetation, it is essential to know the partitioning of water into transpiration and evaporation, runoff and associated water ages. For this purpose, we evaluated how topography and vegetation influence water flux and age dynamics at high temporal (hourly) and spatial (10 m) resolution using the Spatially Distributed Tracer-Aided Rainfall-Runoff model for the tropics (STARR*tropics*). The model was applied in a tropical rainforest catchment (3.2 km^2) where data were collected biweekly to monthly and during intensive monitoring campaigns from January 2013 to July 2018. The STARR*tropics* model was further developed, incorporating an isotope mass balance for evapotranspiration partitioning into transpiration and evaporation. Results exhibited a rapid streamflow response to rainfall inputs (water and isotopes) with limited mixing and a largely time-invariant baseflow isotope composition. Simulated soil water storage showed a transient response to rainfall inputs with a seasonal component directly resembling the streamflow dynamics which was independently evaluated using soil water content measurements. High transpiration fluxes (max 7 mm/day) were linked to lower slope gradients, deeper soils and greater leaf area index. Overall water partitioning resulted in 65% of the actual evapotranspiration being driven by vegetation with high transpiration rates over the drier months compared to the wet season. Time scales of water age were highly variable, ranging from hours to a few years. Stream water ages were conceptualized as a mixture of younger soil water and slightly older, deeper soil water and shallow groundwater with a maximum age of roughly 2 years during drought conditions (722 days). The simulated soil water ages ranged from hours to 162 days and for shallow groundwater up to 1,200 days. Despite the model assumptions, experimental challenges and data limitation, this preliminary spatially distributed model study enhances knowledge about the water ages and overall young water dominance in a tropical rainforest with little influence of deeper and older groundwater.

KEYWORDS
Costa Rica, humid tropics, ReBAMB, tracer-aided modelling, transpiration, water ages, water partitioning

1 | INTRODUCTION

Earth's water fluxes depend on a mosaic of complex atmospheric dynamics, heterogeneous land use patterns (Stoy et al., 2019), vegetation, soil, geology and topography. Stream water fluxes have been much more studied than the fluxes that exit the catchment system via evaporation and plant transpiration (Soulsby, Birkel, & Tetzlaff, 2016). Knowledge about the latter processes is constrained by large uncertainties arising from difficult and costly direct measurements (Jasechko et al., 2013). Plant transpiration is considered the largest terrestrial water flux being globally ~50% of the precipitation that reaches the critical zone (Schlesinger & Jasechko, 2014) and ranging from 35 to 90% of the total evapotranspiration across different biomes (Fatichi & Pappas, 2017). In addition, plant transpiration mostly depends on ecosystem characteristics (Berkelhammer et al., 2016; Fatichi & Pappas, 2017) and water availability, which in turn are linked to soil structure (pore size and storage capacity of the matrix), plant root architecture (Allen, Kirchner, Braun, Siegwolf, & Goldsmith, 2019) and plant physiology (Gotsch, Asbjornsen, & Goldsmith, 2016). Moreover, plant transpiration follows seasonal dynamics and varies in relation to the water intake (Sprenger, Tetzlaff, Buttle, Laudon, & Soulsby, 2018).

Greater water and energy inputs in the humid tropics relative to temperate climates result in rapid rates of change in catchment hydrological processes and flux dynamics (Wohl et al., 2012). However, the partition of precipitation into different fluxes and storages remains poorly understood. A limited quantitative understanding of the role of the tropical vegetation (Stoy et al., 2019) in the hydrological and biogeochemical cycles, as well as regarding time and sources for plant water uptake (Schlesinger & Jasechko, 2014) constrains the assessment of land use change impacts at the catchment scale. To estimate the impact of land use and vegetation changes on the hydrological cycle, and to properly attribute stream changes to anthropogenic induced landscape modifications, high resolution spatial–temporal analysis of flux dynamics in the critical zone is required (Brantley et al., 2017; Evaristo et al., 2019). Ecohydrological processes in the tropics differ dramatically from those in arid landscapes (Aparecido, Miller, Cahill, & Moore, 2017; Moore, Orozco, Aparecido, & Miller, 2018) and other hydroclimatic regions. Out of those processes, particularly the transpiration of tropical rain forests has been poorly explored. Studies have shown that future increase in relative humidity and the length of drought periods may affect transpiration rates, increasing the temperature of the leaves of tropical species and influencing their growth (Feeley, Joseph, Nur, Kassim, & Davies, 2007; Perez & Feeley, 2018). Moreover, as dew deposition is known to suppress transpiration and carbon uptake in leaves (Gerlein-Safdi et al., 2018) and is highly sensitive to changes in temperature and humidity, it can be hypothesized that variations in transpiration rates will be associated with increasing temperature trends in the tropics.

The spatio-temporal evaluation of water ages is essential to better understand how precipitation is partitioned into streamflow and transpiration and their interactions between storage and fluxes in the hydrological cycle (Grant & Dietrich, 2017; Hrachowitz, Savenije, Bogaard, Tetzlaff, & Soulsby, 2013; Sprenger et al., 2018). Water age distributions, characterized by transit time distributions (TTDs) and residence time distributions (RTDs), are informative and widely used in ecohydrological studies (Sprenger et al., 2018). However, process inference from TTD analysis also involves major simplifications like a priori assumed shape of the distribution, which is rarely the case in real-world catchments (Evaristo et al., 2019; Kirchner, 2016). Alternatively, tracer-aided hydrological modelling (commonly using $\delta^{18}O$ and/or $\delta^{2}H$) tools can represent the natural non-stationary behaviour (Birkel & Soulsby, 2016; Rinaldo et al., 2011) of experimental water age distributions without a priori assumptions of TTDs and RTDs, but it requires parameterization of the mixing processes involved (Hrachowitz et al., 2013). This type of model also allows exploration of the movement of water through storage components, and the ecohydrological partitioning of precipitation (Birkel & Soulsby, 2016; Knighton, Saia, Morris, Archiblad, & Walter, 2017; Seibert & McDonnell, 2002). Such knowledge cannot be gained from modelling rainfall-runoff dynamics alone (Birkel & Soulsby, 2015). As such, tracer-aided models have been used to determine suitable model structures derived from hydrometric and tracer information (for a recent review, see, e.g., Birkel & Soulsby, 2015), and to constrain model parameter uncertainty facilitating model evaluation (Birkel, Soulsby, & Tetzlaff, 2014). The multiple interacting pathways (MIPs) model was used to test hypotheses of tracer transport and mixing for a suitable physical representation of subsurface flow paths at the hillslope scale (Davies, Beven, Nyberg, & Rodhe, 2011). Furthermore, the adaptation of StorAge Selection (SAS) functions into hydrological models has been used to assess inter-relationships between soil and vegetation, their fluxes, storage and water age dynamics (Harman, 2015; Smith, Tetzlaff, & Soulsby, 2018). However, the recent development and application of spatially distributed tracer-aided hydrological models enabled the evaluation of the influence of spatial heterogeneity on water transit times (Remondi, Kirchner, Burlando, & Fatichi, 2018), large-scale snowmelt processes and runoff generation (Stadnyk, Delavau, Kouwen, & Edwards, 2013) and the spatially explicit assessment of water storage-flux-age interactions (Ala-aho, Tetzlaff, McNamara, Laudon, & Soulsby, 2017; Dehaspe et al., 2018; Piovano et al., 2019). Despite the high computational demand of distributed tracer-aided models (van Huijgevoort, Tetzlaff, Sutanudjaja, & Soulsby, 2016a), their development can help avoid that spatial aggregation jeopardizes the implementation of more realistic process conceptualization and water age estimations (Kirchner, 2016). Nonetheless, more complex model process representation often comes with an increased number of model parameters that need calibration and potentially lead to larger model uncertainty (Birkel & Soulsby, 2015).

The Spatially Distributed Tracer-Aided Rainfall-Runoff (STARR) model (van Huijgevoort, Tetzlaff, Sutanudjaja, & Soulsby, 2016b), developed to understand internal catchment processes, was applied at diverse temporal and spatial scales. Most of the applications were conducted in northern latitudes where it was used to visualize patterns of connectivity and runoff ages (van Huijgevoort et al., 2016b), and was adapted to climatic conditions with presence of snow (Ala-aho et al., 2017) and permafrost-influenced catchments (Piovano et al., 2019). Furthermore, it was recently adapted to tropical climate and vegetation (STARR model for the tropics; STARR*tropics*) characteristics (Dehaspe et al., 2018). However, the model did not yet include an ecohydrological component of water partitioning and water age tracking.

Spatial and temporal tracer availability as model input data considerably constraints the use of tracer-aided models (Delavau, Stadnyk, & Holmes, 2017). To overcome this issue, we established a hydro-meteorological and isotope data collection network in a pristine tropical rainforest catchment (3.2 km^2) in northern Costa Rica from January 2013 to July 2018. Building on the work by Dehaspe et al. (2018), the collected data were used to conceptualize, drive and evaluate STARR*tropics* at an hourly frequency with a 10 m spatial resolution and water age tracking. Efforts were focused on assessing the role of the rainforest vegetation on water partitioning enhancing model development to track transpiration flux and age dynamics within the STARR*tropics* framework keeping the number of calibrated parameters as low as possible.

With STARR*tropics*, we simulate rainforest interception, transpiration, soil water, groundwater and streamflow and the respective water ages throughout the model cascade, with the following specific objectives:

1. Further develop STARR*tropics* to isotopically partition the evapotranspiration flux into evaporation and transpiration and to enable tracking of water ages.
2. Use the modified model to assess the spatio-temporal variability of water fluxes, storage and water age distributions in relation to topography, soil and vegetation characteristics.

2 | STUDY AREA AND DATA

2.1 | Study site

This study was conducted in the Alberto Manuel Brenes Biological Reserve (ReBAMB) (Figure 1b), a pristine 3.2 km^2 tropical, rainforest headwater catchment (San Lorencito River) in northern Costa Rica, which drains ultimately into the Caribbean Sea. The elevation varies between 874 and 1,472 m.a.s.l. with an average slope of 22% (Dehaspe et al., 2018). The area of study corresponds to a transition region, climatically influenced by the Eastern tropical Pacific Ocean and the Caribbean Sea (Sáenz & Durán-Quesada, 2015). The Caribbean climate is reflected by consistent rain and high relative humidity throughout the year, while the Pacific influence is associated with rainfall events mainly between May and November (Solano-Rivera et al., 2019). Despite being mostly influenced by the Caribbean weather, it is also affected by the decrease in rainfall associated with the Mid Summer Drought (Magaña, Amador, & Medina, 1999). The area receives moist airflow of the Caribbean Low Level Jet (CLLJ, Amador, 2008), the influence of the seasonal migration of the Intertropical Convergence Zone (ITCZ) and the passage of transient systems. The annual rainfall in the study area measured at 967 m.a.s.l. is on average 2,790 mm (2,398–3,372 mm for the period from 2013 to 2017). The monthly rainfall regime exhibits a moderate seasonality with a wet season between May and November and a drier period between December and April. Frequent drizzle and light rain with intensities between 2 and 15 mm/hr are commonly evidenced (Solano-Rivera et al., 2019). Regarding the spatial variability of precipitation, Solano-Rivera et al. (2019) found no significant precipitation elevation gradient within the catchment. The annual reference evapotranspiration ranged from 330 to 580 mm, with a mean air temperature of 19.7°C, and 96.3% of average relative humidity. The average annual discharge is 2,100 mm. Discharge time series (Figure 1a) show a flashy response to rainfall inputs with an overall response time of around 40 min (Dehaspe et al., 2018). The lowest discharge values were observed during the drier months (March and April), with a measured minimum of 0.02 m^3/s (Dehaspe et al., 2018).

Volcanic Andosols and Entosols are the dominant soil types (Figure 1c shows soil profiles of Andosols from the south and north hillslope). The former with depths ranging from about 60 to 150 cm, mostly covers the hillslopes with decreasing soil depth towards the lower part of the catchment close to the mainstem of the San Lorencito stream where Entosols are located. Both are rich in organic matter (~10 to 20%), generally porous and with an infiltration capacity that exceed 1,000 mm/hr (Balzer, Schulz, Birkel, & Biester, 2020; Solano-Rivera et al., 2019). Soil samples taken from the northern and southern slopes showed average values of 4.6 and 5.4 for pH, 0.4 and 0.6 g/cm^3 for bulk density and 77.9 and 69.4% for porosity. These values are the average of samples from five sites on the northern hillslope and four on the southern hillslope at three depths, respectively, 10, 30 and 50 cm. Measurements of clay content reflected an increase with depth (max 20%) reflected in a decrease of saturated hydraulic conductivity with depth. The less developed Entosols at the footslopes, and in the valley bottoms result from material transport and deposition in the catchment. High material transport rates are generated by heavy rainfall that saturates the soil, leading to landslides and erosion even under a pristine forest cover (Solano-Rivera et al., 2019). From a geological perspective, the catchment area is the product of erosive processes and hydrothermal alteration of volcanic and vulcanoclastic rocks (2–9 million years) from the Pleistocene (Denyer & Kussmaul, 2000). Andesitic and basaltic lavas, plagioclases, breccias and tobas are the dominant rocks. Mineralogically, phenocrystals of augite, hypersthene and magnetite and in a smaller proportion hornblende and olivine of the Monteverde Formation are evidenced. The stream geomorphology is typical of a V-form valley mountain torrent controlled by normal parallel faults. According to the life zone classification of Holdridge (1967), our study site is covered by a pristine and dense pre-montane rainforest (Figure 1c, central panel). The dominant tree species are Elaegiaux panamensis and Ocotea morae, palmito (Iriartea deltoidea) and various types of higuerones (Ficus) (Salazar, 2003). Based on in situ observations, fine roots reach down to 1 m. The vegetation height, estimated as the difference between the surface elevation and the digital terrain model (Dehaspe et al., 2018), shows a concentration of the highest trees in the central

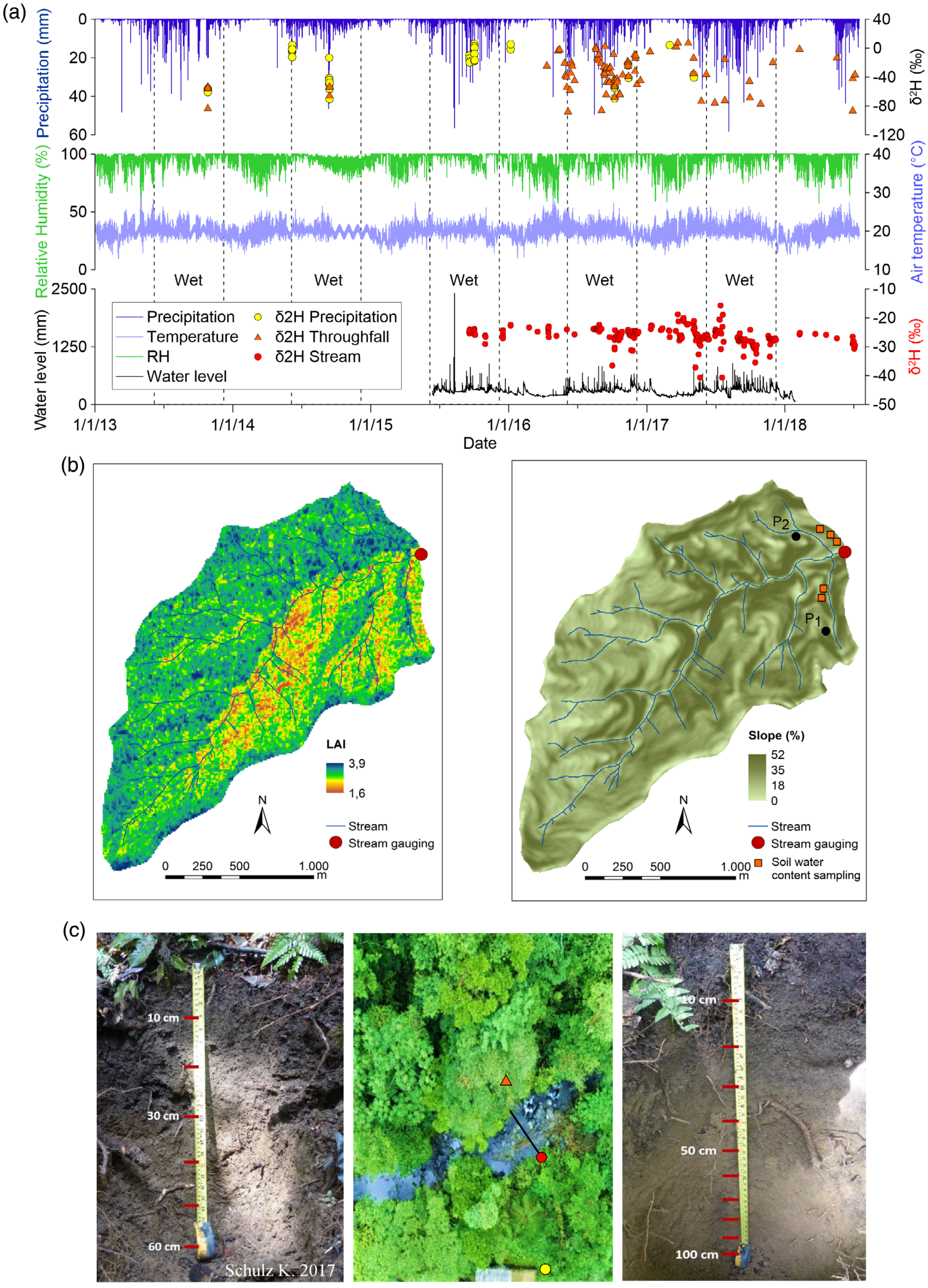

FIGURE 1 Legend on next page.

part of the catchment (approx. 25 m height), while the minimum height in the riparian zone is only at around 2 m (Salazar, 2003). Furthermore, a higher leaf area index (LAI) is evidenced on the northern hillslope of the catchment, which also corresponds to lower slopes and deeper soils in comparison to the southern hillslope (Figure 1b).

2.2 | Hydro-climatic, isotopic and geospatial data

Meteorological data were collected from July 2008 to July 2018 using a Davis Vantage Pro 2 weather station located 1 km outside the catchment (at 967 m a.s.l.). The station recorded: wind speed (±0.1 m/s), relative humidity (±1%), incident solar radiation, temperature (±0.2°C) and precipitation (±0.2 mm) at 30-min intervals. This information was aggregated to 1 hr and used to derive ET estimates for the catchment using Penman-Monteith (Allen, Pereira, Raes, & Smith, 1998). Data gaps (<10%), were filled using a sine wave criterion for temperature and the remaining variables using an average year criterion following Dehaspe et al. (2018). In June 2015, a water level station (Figure 1c, central panel and Figure 1a) was equipped with a Global Water GL-500 water-level sensor (precision of ±5 mm) recording at 5-min intervals. Discharge measurements (n = 104) used for model calibration were conducted manually using a Global Water FP111 current meter (accuracy of 0.05 m/s) and by salt dilution using a multiparameter water quality sensor (Hanna HI98195). Measurements were carried out at biweekly to monthly frequencies from 2013. We also monitored 15-min soil water content at both hillslopes using five multi-depth soil water probes (Odyssey) installed and calibrated with on-site soil material for 20 cm depth increments (10, 30, 50, 70 and 90 cm) over the rainy season in 2017 (Figure 1). The measurement unit was mm per 10 cm soil depth directly converted using soil texture and porosity data from manual soil samples at the sites of installed soil water probes.

Water samples for isotope analysis were collected manually in precipitation, throughfall and stream water on a biweekly to monthly resolution. Furthermore, stream water samples (in total n = 270 at the outlet) were collected almost daily using an ISCO 3700 automatic water sampler from 2016 to 2018 and manually during intense (15-min) field campaigns (Figure 1a). The monitoring period for isotope samples ran from January 2013 to July 2018. Precipitation and throughfall samples were collected using a 3-l plastic bottle through a funnel and inlet tube, Palmex Rain Sampler RS1, to prevent evaporation in cumulative samples (Gröning et al., 2012). Water samples were stored in 50-ml polypropylene bottles, sealed with screw caps and later stored in a fridge at 5°C until analysis. Samples were filtered through 0.45-μm polypropylene membrane filters (Puradisc 25PP Whatman Inc., Clifton, NJ, USA) to minimize organic matter contamination. The isotopic composition ($\delta^{18}O$ and δ^2H) of the samples was determined at the laboratory of the Isotopes Research Group, Universidad Nacional de Costa Rica (UNA-SIL), using a Cavity Ring Down Spectroscopy (CRDS) water isotope analyser L2120-*i* (Picarro, USA) and a LWIA-45-EP water isotope analyser (Los Gatos, USA). $^{18}O/^{16}O$ and $^2H/^1H$ ratios are presented in delta notation δ (‰), with reference to the VSMOW-SLAP scale. Calibrated secondary standards were used to normalize the results as well as to assess quality and drift control procedures (Sánchez-Murillo et al., 2019). The analytical long-term uncertainty was: ± 0.5 (‰) (1σ) for δ^2H and ± 0.1 (‰) (1σ) for $\delta^{18}O$. All the results were processed using the ChemCorrect 1.2.0 software (Picarro, Sunnyvale CA, USA) (Picarro, 2010) to detect organic acid and alcohol sample contamination. Due to the high collinearity between δ^2H and $\delta^{18}O$ (R^2 > 0.9), only δ^2H was selected for modelling.

The model requires as input, a continuous hourly time series for isotopic composition of precipitation. Following Dehaspe et al. (2018), a multiple Linear Regression (MLR) model (δ^2H = −222 + 3.5(wind speed) + 1.9(relative humidity); adjR^2 = 0.3) was implemented to derive the isotope composition of rainfall above canopy level using the R package *packfor* (Dray, Legendre, & Blanchet, 2009). Spatial 10 m pixel size maps used as model input are: Digital Elevation Model (DEM), Digital Surface Model (DSM), LAI and Topographic Wetness Index (TWI). The DEM and DSM were used to represent vegetation height. LAI depicts the leaf area per unit ground surface (Zheng & Moskal, 2009) and TWI as a function of specific contributing area and local slope angle (Beven & Kirkby, 1979) was used to represent the distributing runoff generation mechanisms.

3 | MODEL DEVELOPMENT

3.1 | Model structure

The STARR model, built in the PCRaster python framework (Karssenberg, Schmitz, Salamon, de Jong, & Bierkens, 2010) and based on a HBV-type conceptualization (Hydrologiska Byråns Vattenbalansavdelning; (Seibert & Vis, 2012), was developed by van Huijgevoort et al. (2016a) to better account for internal catchment processes incorporating tracer mixing and flux tracking at a daily time step and over a 100 m grid.

The modified STARR*tropics* model of Dehaspe et al. (2018) uses hourly input time series of precipitation, evapotranspiration, temperature and the δ^2H composition of precipitation to simulate water fluxes, storage dynamics, and isotope ratios through a cascade of

FIGURE 1 The San Lorencito River catchment located in the Reserva Biológica Alberto Manuel Brenes (ReBAMB), northern Costa Rica. (a) Average hourly hydro-climatic data and isotope (δ^2H) compositions of precipitation, throughfall and stream water for the study period (January 2013–July 2018). The dotted lines separate wet and dry seasons. (b) Leaf Area Index (LAI) and slope (%) maps at 10 m grid size, orange squares represent the soil water content sampling sites and (c) aerial image of the typical vegetation cover, stream gauging section (black line), water level monitoring site (red circle) precipitation sampling site (yellow circle) and throughfall sampling site (orange triangle) with south and north hillslope Andosol soil profiles (courtesy of Katrin Schulz) model components. For the interception module, the assumption that the canopy dries completely between events (Hoelscher, Koehler, van Dijk, & Bruijnzeel, 2004) was considered. Therefore, the Rutter model (Rutter, Kershaw, Robins, & Morton, 1971; Rutter, Morton, & Robins, 1975) was applied to the incoming rain at canopy level, using an empirically estimated canopy gap of 5%. Furthermore, to account for fractionation in the interception module, an empirical relationship between precipitation and throughfall was considered to estimate the consistently enriched isotope signatures of throughfall (Dehaspe et al., 2018). The distribution of water in the different soil layers varies according to the water retention capacity of the soils, which in turn is a function of the proximity of the model grid cell to the stream, distinguishing the riparian zone from the hillslopes. The unconfined groundwater storage was represented as a linear reservoir generating discharge and the lateral flow based on Darcy's Law (Darcy, 1856). The streamflow generation represents the integration of the flows through each module and cell per time unit. Additionally, the tracking of isotope composition through the different model storages is based on an isotope mass balance connected to the water fluxes. We refer to Dehaspe et al. (2018) for a detailed description of the model structure, and equations. A table with fixed and initial parameter ranges, as well as the calibrated best fit parameter set, is presented in Table 1.

3.2 | Transpiration

In order to quantify the disaggregation of evapotranspiration into transpiration and evaporation in our very humid and energy-limited study site with no dual isotope plot evidence of evaporative fractionation in streamwaters, we used the following basic assumptions:

1. Transpiration is a non-fractionating process (Chakraborty, Belekar, Datye, & Sinha, 2018).
2. Plant water uptake uses non-fractionated soil water (a valid approximation according to Ferretti et al. (2003) and Sutanto, Wenninger, Coenders-Gerrits, and Uhlenbrook (2012)).
3. Un-observed isotope composition of evaporating water is directly related to environmental variables (temperature and relative humidity) according to Gibson, Birks, and Edwards (2008).

Therefore, in absence of in-situ water vapour, soil and xylem isotope measurements, we modified STARR*tropics* to include a simplified version of the Craig-Gordon model (for the liquid phase of soil water) to compute the isotopic composition of the evaporating flux (δ_E). We assumed the residual liquid (δ_L) to be the isotopic composition of precipitation and δ_E was estimated using Equation (1) (for a detailed discussion on this assumption we refer to, for example, Gonfiantini et al., 2018):

$$\delta_E = \frac{1}{1-h+\varepsilon_K}\left(\frac{\delta_L-\varepsilon^+}{\alpha^+}-h\delta_A-\varepsilon_K\right) \tag{1}$$

In Equation (1), h represents the relative humidity, ε^+, the equilibrium isotopic separation factor between liquid and vapour, and is calculated as $\varepsilon^+ = \alpha^+ - 1$. α^+ is the liquid–vapour equilibrium isotopic fractionation factor, estimated for δ^2H from empirical relations as follow: $1{,}000 \ln\alpha^+ = 1{,}158.8(T^3/10^9) - 1{,}620.1(T^2/10^6) + 794.84(T/10^3)$

TABLE 1 STARR*tropics* model parameters, units, fixed and initial ranges and calibrated best fit parameter set

Parameter	Unit	Description	Fixed-initial range	Best fit
Evapotranspiration				
zh	m	Height above ground of humidity measurement	2	
zm	m	Height above ground of windspeed measurement	10	
rl	mm/s	Stomatal resistance	140	
Interception				
DS	mm/hr	Drainage from canopy when the storage is completely filled	0.08–0.12	0.082
b	–	Exponent in Rutter interception module	3.7–5.1	4.751
Soil storage				
FC1	mm	Water holding capacity of the soil in hillslopes	100–500	206.432
FC2	mm	Water holding capacity of the soil in valleys	1–100	19.188
beta	–	Non-linear exponent for soil store runoff generation	0.01–4	2.724
ks	1/hr	Recession coefficient discharge from soil store	0.0042–0.021	0.009
STOpas	mm	Passive soil storage	1–300	146.206
fracSTO	–	Differentiates passive storage in valley and hillslope	0–1	0.788
Groundwater storage				
kg	1/hr	Recession coefficient for discharge from groundwater store	0.000042–0.0042	0.001
ksat	mm/hr	Horizontal saturated hydraulic conductivity	0.0000042–8	5.586
Gwpas	mm	Passive groundwater storage water	0–1,000	819.116

$- 161.04 + 2.9992(10^9/T^3)$ (Horita & Wesolowski, 1994), T, expresses temperature in Kelvin degrees. ε_K, represents equivalent kinetic isotopic separation factor $\varepsilon_K = nC_K^{\circ}\theta(1-h)$ where n = 1/2 for open water bodies, C_K° is 25 ‰ for δ^2H data, and $\theta \approx 1$ for small water bodies (Gonfiantini, 1986). The δ_A is the isotopic composition of ambient atmospheric vapour computed using the precipitation-equilibrium assumption (Gibson et al., 2008) with δ_P as the isotopic composition of precipitation values (Equation (2)):

$$\delta_A = \frac{(\delta_P - \varepsilon^+)}{\alpha^+} \tag{2}$$

The evapotranspiration (ET) was computed based on the FAO Penman-Monteith standard approach (Allen et al., 1998). We assumed that ground radiation loss is a fraction of the incoming net radiation and that the net long-wave night radiation flux is equal to the net long-wave radiation 2 hr before the sunset of the corresponding day (Dehaspe et al., 2018). The ET was evaluated considering surface resistance, which is a key constraint in tropical regions where radiation and wind effects must be accounted for. Moreover, a local mass balance was implemented for the calculation of transpiration. $ET = E + Tr$, where E represents evaporation and Tr, transpiration. To derive Equation (3), it was additionally assumed that the isotopic composition of ET is δ_A (Equation (2)), of E is δ_E (Equation (1)) and of Tr is δ_S, respectively. The δ_S corresponds to the simulated isotopic composition of soil water as the main source of plant water uptake. Tr was therefore calculated for every cell at each time step as follows:

$$Tr = ET\frac{(\delta_A - \delta_E)}{(\delta_S - \delta_E)}. \tag{3}$$

The range 0 < Tr < ET was restricted to avoid unreasonable Tr values that are theoretically possible when $\delta_A > \delta_E$ and $\delta_S < \delta_E$. The δ_E is always more depleted compared to δ_A with our data set, but transferring this approach needs careful consideration.

We analysed the spatial variability of transpiration between northern and southern hillslopes evaluating simulated spatial maps and time series extracted at individual cells on each of the two hillslopes P1 (south) and P2 (north) and the ages of the stream, respectively (Figure 1). Following van Huijgevoort et al. (2016a), water ages were spatially and temporally tracked for every cell assuming a complete and instantaneous mixing in storages and fluxes. A flux tracking approach was used according to Hrachowitz et al. (2013) and Birkel and Soulsby (2015), where a label was assigned with a time stamp to each incoming rain and the increasing age of waters moving through the model cascade tracked to give a final age label at the exit of the catchment in hours. Resident water in storage increases its age before contributing to the stream or exiting the catchment via evapotranspiration (water stored in each cell becomes 1 hr older). For the particular case of transpiration, we considered two alternatives of modelled age dynamics reflecting the full range of possible water ages resulting from model assumptions based on Sprenger et al. (2019):

1. In the first case, we assumed that the water for transpiration is taken from the shallowest layer of the soil starting from zero counts of the age tracking.
2. In the second case, water uptake from deeper soil depths is allowed by labelling the initial transpiration with the age of the shallow soil water at that specific time step.

These two alternative cases allow consideration of the upper and lower age boundaries of the transpiration flux. We mechanistically interpret the first case representing saturation conditions mainly occurring during the rainy season from April to December and nearly negligible mixing with water previously stored in the soil, whereas the second involves infiltration processes and complete mixing with resident water of deeper soil horizons.

3.3 | Model evaluation and calibration

We used a 1-year warm-up period (2013 looped twice) to avoid initialization errors for a uniform Monte Carlo parameter sampling approach. A total of 2,131 simulations with a run time of 2 weeks were performed using six available nodes from the *Tsaheva* High Performance Computing system at the Geophysical Research Center of the University of Costa Rica to test the model skill with a random parameter set, while other parameters were fixed (3 fixed and 11 calibrated parameters) based on previous model experiments (Table 1). Model evaluation of outputs used the manual streamflow gauging (104) and isotope measurements (270). In addition, an independent and qualitative model evaluation of simulated soil water storage with soil water measurements collected at 0.5 m below ground (Figure 1) over the rainy season from June 2017 to November 2017 (Figure 3) was carried out. The simulations were accepted based on the following multiple criteria:

1. For the annual water mass balance, only discharge simulations that do not exceed 10% variation of precipitation minus total ET for any simulated year were accepted (Dehaspe et al., 2018).
2. The simulated discharge cannot be lower than the observed minimum of 0.02 m^3/s.
3. For discharge, only the Nash-Sutcliffe (NSE) and Kling-Gupta Efficiencies (KGE) (Gupta, Kling, Yilmaz, & Martinez, 2009) above zero (Nash & Sutcliffe, 1970) were retained.
4. Finally, from the retained runs, the mean absolute error (Willmott & Matsuura, 2005) was used to evaluate the δ^2H stream simulations named hereafter MAEiso. Simulated runs with MAEiso <3 ‰ were accepted. In the MAEiso the estimates of the error range are in the same units as the variability of the observations. This index was chosen since it minimizes the bias between observations and simulations in contrast to other statistics that emphasize variability and correlation (Ala-aho et al., 2017; Piovano et al., 2019).

Due to the spatial complexity (10 × 10 m cells) and the period considered between January 2013 and July 2018 (48,500 hourly time steps), the model run time increased to almost 17 hr, which limited the ability to perform a formal uncertainty analysis. Therefore, we constrained our analyses to the number of simulations retained after satisfying all the above criteria.

4 | RESULTS

4.1 | The STARR*tropics* simulated streamflow and stream isotopes

Discharge simulations (from 142 retained runs) reasonably captured high and low flows, flood peaks and the subsequent recession curves (Figure 2a). Moreover, the model was able to capture the flashy catchment response to heavy rainfall events, as well as the streamflow seasonality. Accepted simulations resulted in a best-fit of 0.69 for NSE and 0.67 for KGE. From these simulations, the runs with the MAEiso <3 ‰ (12 runs) are presented in Figure 2b. Similarly, stream isotope simulations captured the isotopic dynamics and the best-fit simulation resulted in a minimum MAEiso of 2.3 ‰. Simulations of δ^2H matched the mostly invariant baseflow isotope composition of observed values (between −20‰ and − 30‰) over the entire monitoring period. For the study period, only two isotope events (≈ −40‰) in May and June 2017 were not fully captured by the model. As an independent, qualitative model evaluation (Figure 3), the output time series from the soil storage module were plotted against the in-situ soil water measurements at 50 cm depth. The simulations captured the behaviour of the transient soil water storage dynamics and both the optimal model simulations and averaged in-situ measurements, gave similar median values of 32 and 36 mm, respectively (Figure 3 inlet boxplot). Although the simulations overestimated peaks and underestimated lower soil water content, the model matched the overall soil water dynamics.

4.2 | Simulated spatio-temporal transpiration dynamics

Time series of actual evapotranspiration and simulated transpiration from the optimal model run (simulation that satisfies the criteria set out in Section 3.2) at the catchment outlet are presented in Figure 4a. From January 2013 to July 2018, transpiration accounted on average for 65% (percentile (p) p_{25} = 51% and p_{75} = 72%) of the actual evapotranspiration. The average transpiration values in our pristine rain forest catchment were 0.86 mm/day or 288 mm/yr. From a seasonal perspective, greater transpiration was observed in the dry season (December–April), compared to the wet season (May–November), on average, 32 mm/month and 19 mm/month, respectively. Both fluxes indicated a seasonal regime depending on the hydro-climatic conditions. Greater transpiration rates occurred during the dry period and during the transition to the first part of the rainy season. In contrast, lower values were observed during and at the end of the rainy season, with exceptional cases in February and March 2014, where low values were evidenced in near absence of precipitation. Maximum transpiration rates integrated at the catchment outlet reached around 7 mm/day with a larger incidence of high values in the dry period of 2018 compared to previous years. Overall, results evidenced a greater transpiration rate on the northern hillslope compared to the southern hillslope (Figure 4b). The southern hillslope transpiration represented 42% (p_{25} = 32% and p_{75} = 50%) of the transpiration on the northern hillslope derived from the selected points P1 and P2 (Figure 4c). Nevertheless, both transpiration rates followed similar temporal dynamics. The transpiration from P1 accounted for 61% (p_{25} = 54% and p_{75} = 68%) of the transpiration at the outlet and the latter 69% from P2 (p_{25} = 61% and p_{75} = 73%).

The spatially distributed transpiration maps (Figure 4c) showed differences between the hillslopes, particularly during drier conditions (Figure 4c; right panel). Average transpiration rates of 0.45 and

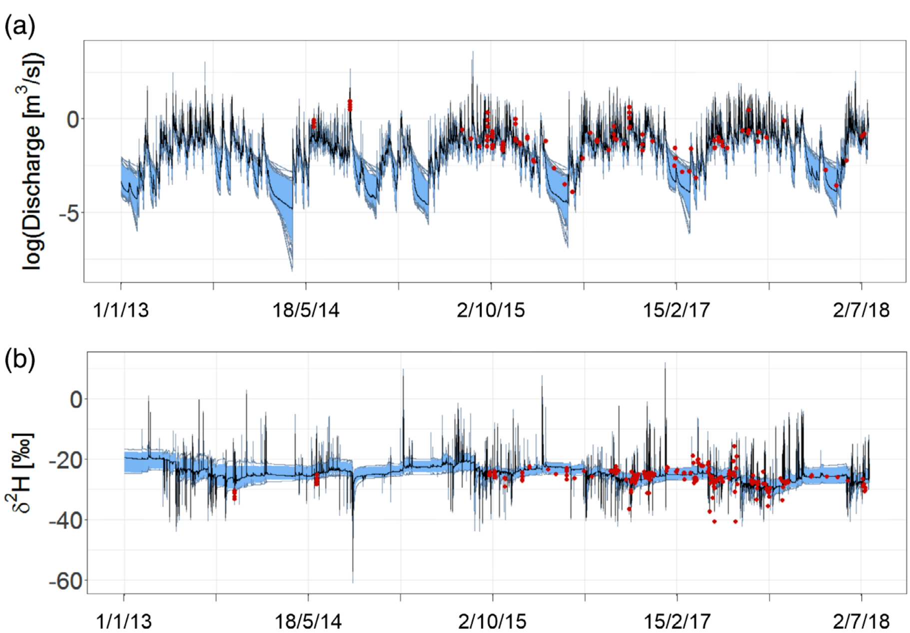

FIGURE 2 The simulated San Lorencito output of (a) discharge (m^3s^{-1}) and (b) stream water isotope compositions; δ^2H (‰). Time series of simulated (grey) and observed (red dots) discharge are plotted on a logarithmic scale, the black line represents the optimal simulation in both cases with the Q_5–Q_{95} percentile range of accepted runs represented as the light blue band

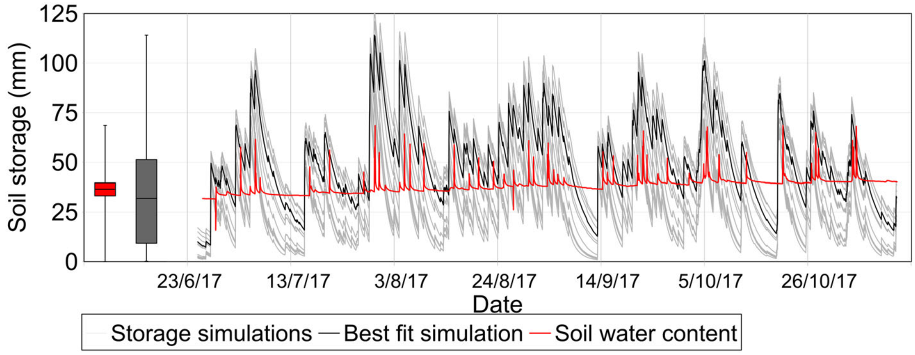

FIGURE 3 Time series of simulated soil storage output used for independent evaluation against soil water content. Time series of simulations (grey) and observed (red line) soil water with the black line representing the optimal simulation. The inlet boxplot of soil storage distributions shows the red box from observed soil water and the dark grey box from the accepted simulations

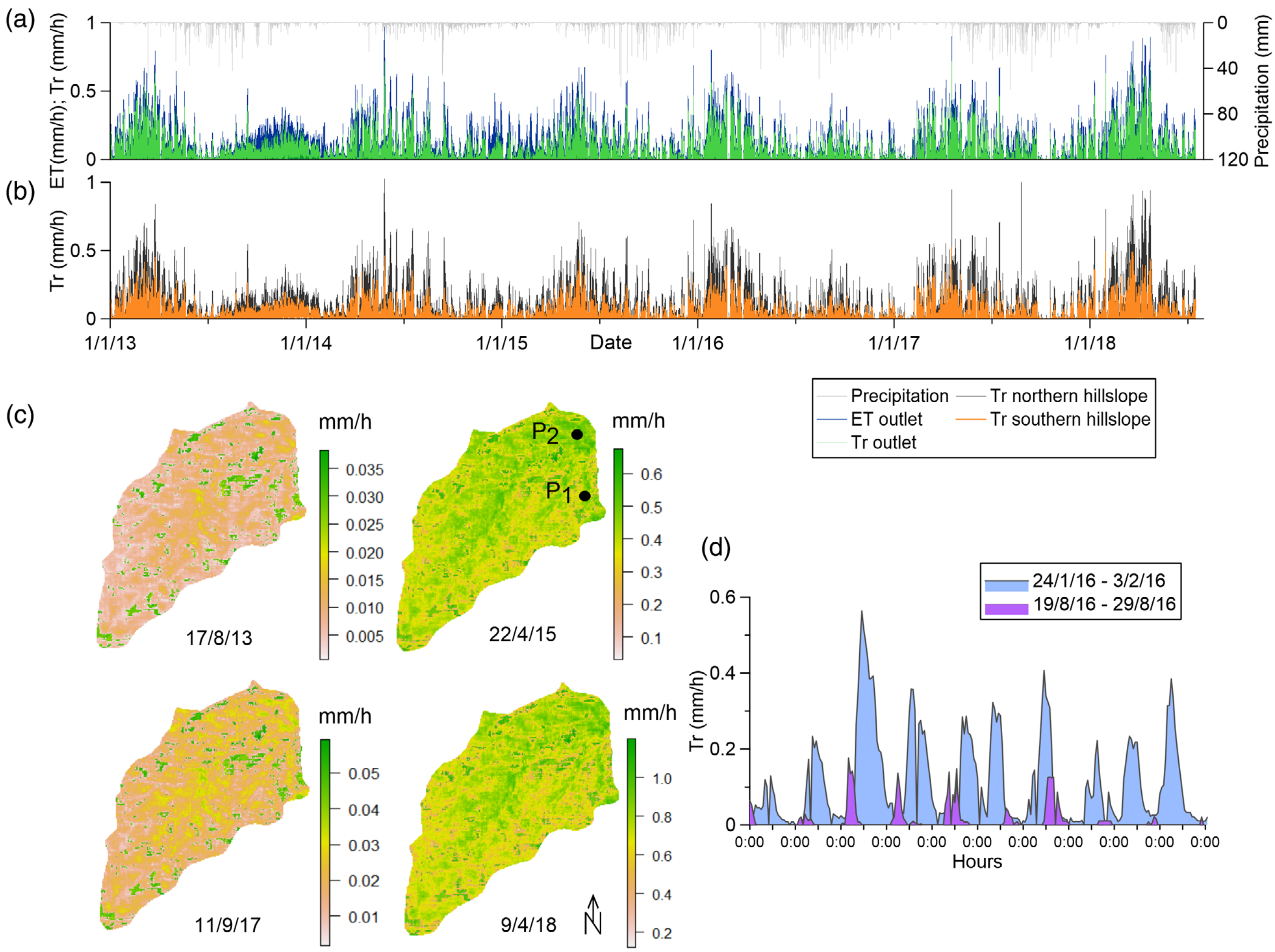

FIGURE 4 (a) San Lorencito hourly simulated time series of actual evapotranspiration (ET), transpiration (Tr) and precipitation for the catchment outlet. (b) Simulated time series of transpiration at P1 (10.2192, −84.5975) and P2 (10.221, −84.5985), respectively, northern and southern hillslopes. (c) Spatial distribution of transpiration for wet (17/08/2013, 11/09/2017) and dry (22/04/2015, 09/04/2018) conditions. (d) 10-days transpiration time series for wet (19/08–29/08, violet) and dry (24/01–03/02, light blue) conditions. Model outputs were extracted from the optimal model run

0.8 mm/hr separated the northern (higher *Tr* rates) from the southern hillslope (lower *Tr*). Also, high transpiration was simulated in the direction of flow towards the lower catchment. Under wet conditions, this difference is less evident and more homogeneous transpiration values were observed over the entire catchment (Figure 4c; left panel). Additionally, we found "transpiration hot spots" showing higher transpiration rates compared to the rest of the catchment.

To check for physical consistency in our high-temporal resolution analysis (Figure 4d), we inspected the catchment diurnal transpiration dynamics for two specific dry and wet periods in 2016 (dry:

24/01–03/02 and wet: 19/08–29/08). Reassuringly, the model reproduced the expected diurnal cycle of higher values during the day reaching peak values around noon and close to zero transpiration at night. Greater values were observed in dry conditions compared to the wet period.

4.3 | The simulated spatio-temporal dynamics of water flux ages

Time series of water age from the different model components at the catchment outlet are presented in Figure 5a, frequency histograms in Figure 5b and in Figure 5c the empirical cumulative distribution functions (CDF). Considering the first case (water for transpiration is taken from the shallowest soil layer with limited pre-event water mixing) of the modelled age of transpiration (subsequently named shallow transpiration), the results showed the best-fit derived shallow transpiration (green line) as the youngest water in the hydrological system reaching 280 hr (~ 12 days) at most. Shallow transpiration ages showed seasonal variation that increased in the periods of less precipitation and vice versa (Figure 5a). The heavily skewed frequency histogram showed that ages between 0 and 10 hr (Figure 5b) were the most common and that almost all observations were younger than 30 hr as also evidenced in the time series. The CDF exhibited logarithmic cumulative patterns with a fast recovery at younger ages for shallow transpiration (Figure 5c). Selecting the 90th and 10th percentile of the distributions, the ages of shallow transpiration did not exceed 20 hr.

Water from the soil (red line) reached maximum ages of 3,890 hr (~ 162 days) and presented a relatively stable dynamic and low seasonality, with 30 days old water as the youngest during rainy periods (Figure 5a). The frequency histogram showed a wider range of ages compared to transpiration. Here a bimodal distribution was observed with peaks of 1,900 and 3,200 hr (Figure 5b). Figure 5c showed a moderately linear behaviour for soil water ages with 90th and 10th percentile values of 3,190 and 1,300 hr.

The stream water ages (blue line) composed from the last two water sources exhibited maximum values of 17,350 hr (~ 722 days) with most occurrences between 2,000 and 3,000 hr. The ages of the stream water responded rapidly to precipitation. Young stream water

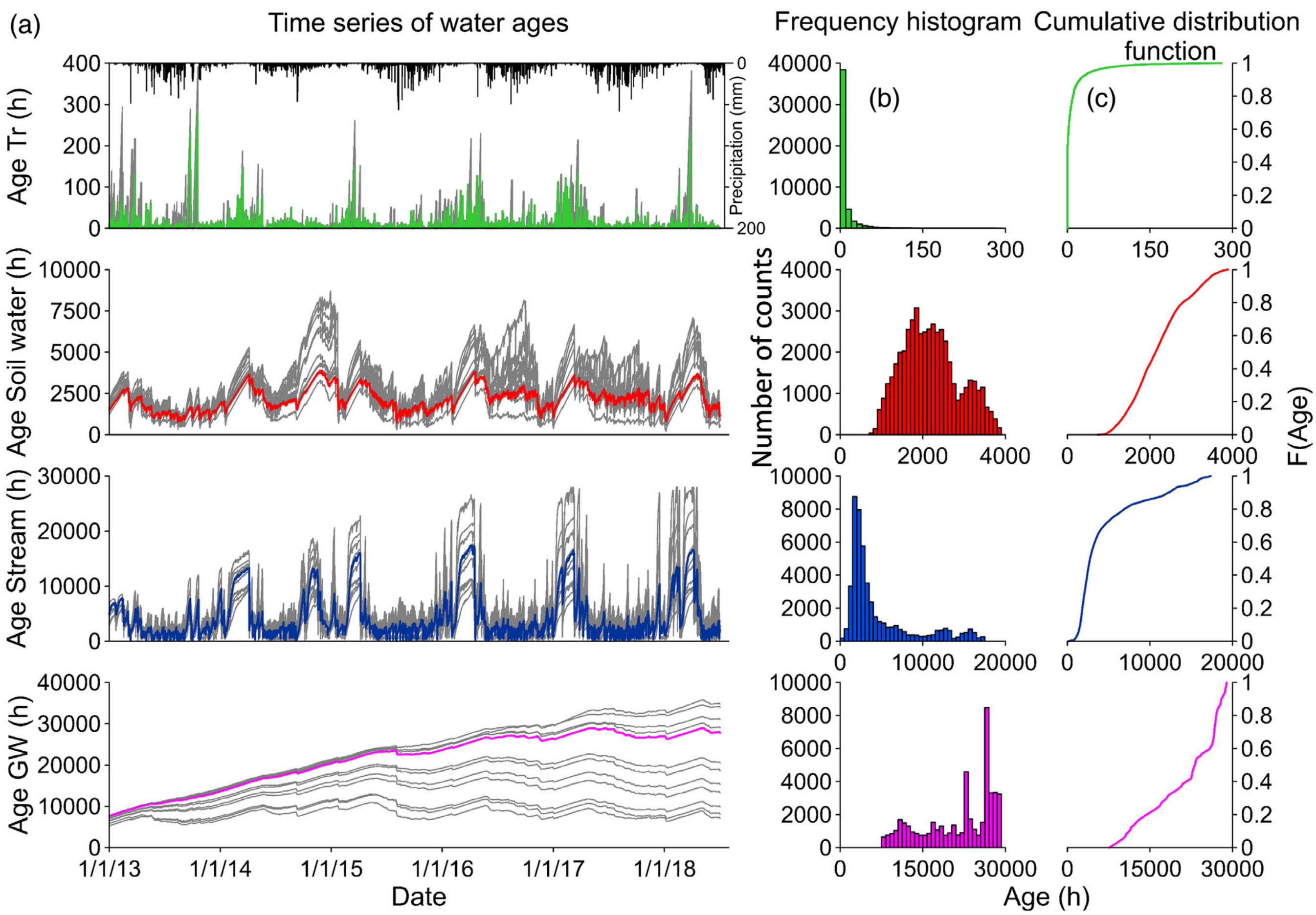

FIGURE 5 Time series of water age simulations of (a) shallow transpiration (Age Tr), soil water (Age Soil water), stream (Age stream) and groundwater (Age GW) from January 2013 to July 2018. (b) Frequency histograms with bin width of 10, 100, 500 and 750 hr for Age Tr, Age Soil water, Age stream and Age GW, respectively. (c) Cumulative distribution functions of water ages for Age Tr, Age Soil water, Age stream and Age GW. Grey lines represent accepted model simulations and the coloured lines the optimal simulation in each case

during the rainy season was in the order of a hundred hours, however during the dry season the age increased to a thousand hours old (Figure 5a). Ages between 2,000 and 3,000 hr were the most frequently simulated within the positively skewed distribution (Figure 5b). The empirical cumulative distribution function of stream (CDF) showed a logarithmic cumulative pattern with a quick response at younger ages. The 90th and 10th percentile were 12,020 and 1,500 hr.

The time series of groundwater ages (magenta line) exhibited a maximum value of 28,930 hr (~1,200 days) and demonstrated lower variability compared to all previously mentioned waters. From 2016 (variations from 25,000 to 30,000 hr), the time series stabilized, and dynamics were moderately influenced by young recharging waters resulting in older ages at the end of the dry season. Earlier (2013–2016), the linear rise pattern in the time series indicates that the model's warm-up period may be longer and do not have implications in the hydrological functioning of the catchment, this issue was evident in this particular component. The ages between 23,000 and 27,000 hr were the most frequently simulated in the negatively skewed distribution (Figure 5b). The CDF exhibited a moderately linear behaviour for groundwater and percentile values of 27,900 and 10,900 hr.

The time series of transpiration age simulated using the second model alternative (water uptake from deeper soil depths with complete pre-event water mixing, subsequently named deep transpiration) were not included in Figure 5 due to the similarity to soil water ages. However, their spatial distribution is presented in the next section.

Figure 6 shows spatial maps of the simulated mean flux age of transpiration, soil and groundwater. The shallow transpiration map (Figure 6a) resulted in slightly lower mean flux ages on the northern hillslope compared to the southern slope. Longer transpiration flux ages were detected close to the catchment boundary and near-zero values in potentially uncovered vegetation areas. The mean deep transpiration flux ages (Figure 6b) showed a different trend with higher values close to the riparian zone (2–5.6 months) and lower ages at the catchment borders (1.5–2 months). The latter followed a similar mean water age pattern of soil water as shown in Figure 6c. Greater mean water age (>5.6 months) reflected potentially disconnected depressions distributed over the catchment. Groundwater mean age varied from 9 to nearly 40 months. Longer residence times were evident in the valley area (31–39 months) and shorter MRTs in the upper catchment area (16–23 months).

5 | DISCUSSION

5.1 | How well does the spatially distributed STARR*tropics* model simulate water, isotope and age dynamics?

Knowledge about the eco-hydrological functioning of tropical catchments is important due to the provision of important ecosystem services (Birkel et al., 2016), their high sensitivity to moisture supply from oceanic water bodies (Durán-Quesada, Gimeno, & Amador, 2017; Munksgaard et al., 2015; Sánchez-Murillo et al., 2016), drought periods (Hidalgo, Amador, Alfaro, & Quesada, 2013) and implications of land use change (Evaristo, Jasechko, & McDonnell, 2015; Ochoa-Tocachi et al., 2016; van Meerveld, Zhang, Tripoli, & Bruijnzeel, 2019). Overall STARR*tropics*, now modified for stream and transpiration water partitioning, facilitates estimation of plant transpiration rates quantifying water age dynamics within the catchment in space and time (McDonnell & Beven, 2014). Our model showed reasonable streamflow performance with best-fit NSE =0.69 and KGE =0.67. The stream isotope composition presented a minimum MAEiso of 2.3‰, indicating that the dominant processes were effectively simulated, and the parameters constrained (Table 1). Similarly, model performance regarding to discharge and stream isotopic simulations was comparable with a previous preliminary application conducted by Dehaspe et al. (2018) using more limited data compared with this study (streamflow measurements 65 vs. 104 and stream isotope samples 73 vs. 270). The model was also comparable to a more parsimonious lumped model simulating TTD and stream isotopes dynamics in the humid tropics of southern Costa Rica (Birkel et al., 2016). Despite the restricted high frequency (monthly and field-campaign based) isotope information, and the use of a MLR model (Dray et al., 2009) to derive input data, STARR*tropics* performed similarly well compared to other applications with measured daily or sub-daily isotope datasets (Ala-aho et al., 2017; Piovano et al., 2019). Such comparability gives confidence in the simulated temporal dynamics of discharge and stream isotopes as well as the mean flux ages estimated for transpiration and different waters within the catchment (Ala-aho et al., 2017). Additionally, independent model evaluation of simulated soil storage dynamics with averaged soil water measurements further increased confidence in our findings (Birkel et al., 2014; Kuppel, Tetzlaff, Maneta, & Soulsby, 2018). However, uncertainties due to data errors, spatially distributed model architecture, model assumptions related to isotope fractionation and the fact that soil physics were not explicitly parametrized in the model cannot be neglected and limited the capability of the model to capture, for example, the most extreme measured peak discharge (Dehaspe et al., 2018). Therefore, following Westerberg and Beven (2011), we directly used manual flow gauging for effective calibration avoiding unnecessary rating curve errors as shown by, for example, Seibert and Beven (2009). More detailed field data in form of atmosphere, soil and plant isotope data will be necessary to further challenge the model assumptions related to ET partitioning made at this stage.

5.2 | How does topography and vegetation influence simulated transpiration fluxes?

The estimated plant transpiration rate from our study is consistent with the now widely accepted concept that transpiration accounts for the largest flux of water to the atmosphere (Jasechko et al., 2013; Schlesinger & Jasechko, 2014). Our findings resulted in an average transpiration of 65% of the total actual ET flux, which is close to that

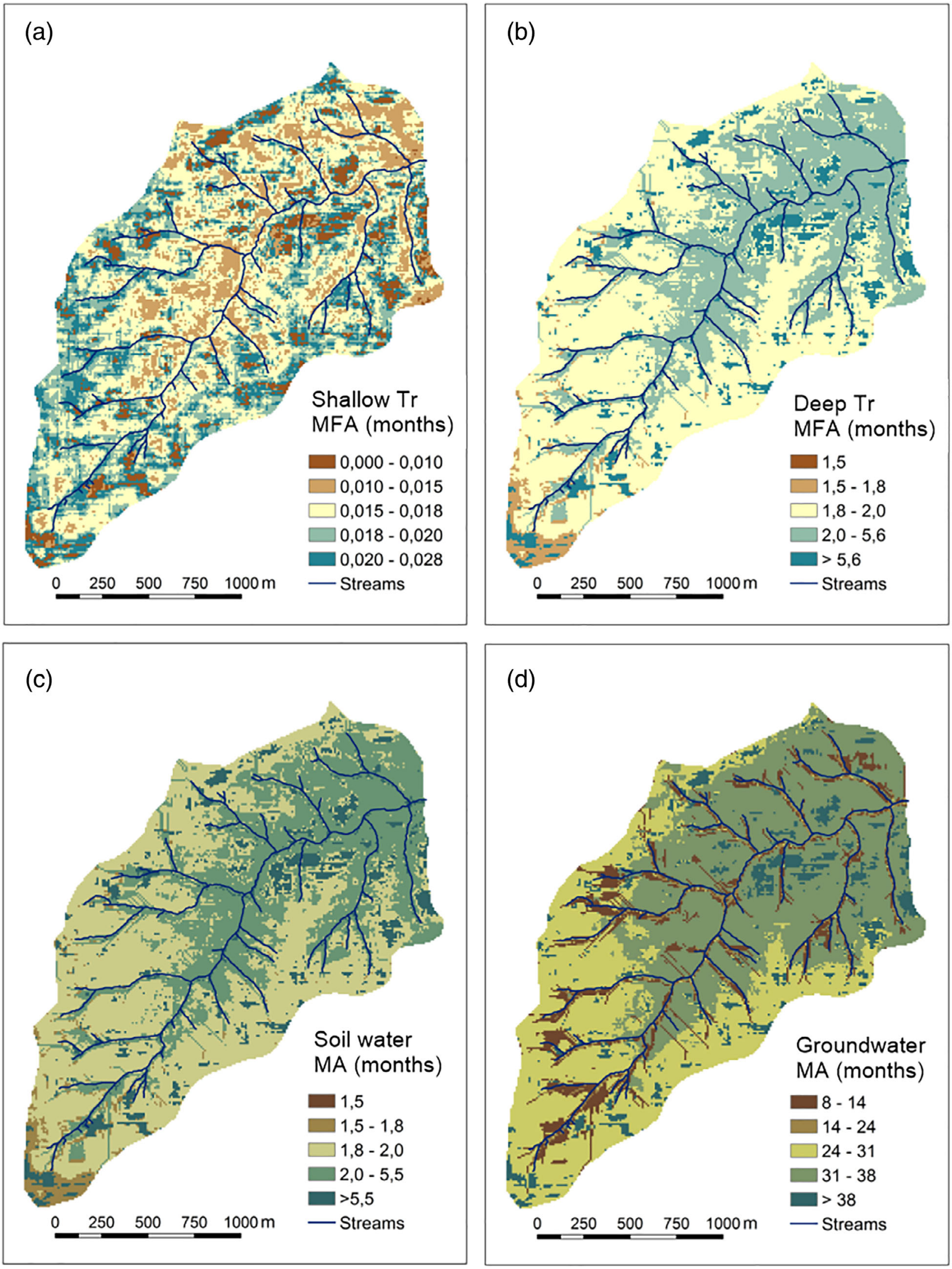

FIGURE 6 The spatial variability of the simulated mean flux age (MFA) and mean water age (MA) computed over the study period: (a) shallow transpiration (Shallow Tr), (b) deep transpiration (Deep Tr), (c) soil water and (d) groundwater (GW) mean age from January 2013 to July 2018. All maps are given at a 10 m × 10 m pixel size and different scales in months

noted by Schlesinger and Jasechko (2014) for tropical forest transpiration (70%). The average annual transpiration flux accounted for 288 mm (p_{25} = 258 mm and p_{75} = 296 mm), which is similar to values reported for a tropical forest catchment in Madagascar (Ghimire et al., 2018) and is also in the range established by Bruijnzeel and Veneklaas (1998) for a tropical montane forest (250–645 mm/yr). However, our daily simulated values were slightly lower compared to measured transpiration in several trees in a nearby, but much wetter (mean annual rainfall >5,000 mm) low montane rainforest catchment (1.4 ± 0.7 mm/day) using heat dissipation sap flow sensors (Moore et al., 2018). The dense vegetation from our catchment together with meteorological variables such as a constantly high relative humidity (98%) and reduced solar radiation due to higher cloud fraction (Dehaspe et al., 2018) may keep the canopy and leaves wet for long time periods, suppressing high transpiration rates (Aparecido, Miller, Cahill, & Moore, 2016; Berry, Gotsch, Holwerda, Muñoz-Villers, & Asbjornsen, 2016).

Seasonal transpiration dynamics (Figure 4a,b) showed a response to climatic conditions and environmental variables, where transpiration remained lower in wet periods and higher over drier months from January to April. Solar radiation and vapour pressure deficit (inversely related to relative humidity) were found in several studies to drive transpiration rates in the tropics (Aparecido et al., 2016; Berry et al., 2016; Moore et al., 2018) together with soil water availability (Ghimire et al., 2018) and leaf temperature (Perez & Feeley, 2018). During water deficit periods, plants tend to close stomata to avoid embolism (Meinzer, Goldstein, Holbrook, Jackson, & Cavelier, 1993). However, at the "evergreen" San Lorencito site, over the period of observations, the catchment did not experiment a marked soil water deficit below 10 cm depth even at the end of the drier months in April (Figure 3), which was evidenced by higher transpiration rates during drier and more cloud-free periods related to increased energy inputs. Overall, diurnal transpiration cycles (Figure 4d) in dry conditions, reached maximum values at noon and low values in the early morning and late afternoon, pointing in the direction of incoming solar radiation influence (Moore et al., 2018). However, in wet conditions we observed substantial differences, with less transpiration and no diurnal pattern due to intermittent cloud coverage (Aparecido et al., 2016). Despite the many simplifying assumptions behind the Tr/ET mass balance, the estimated *Tr* fluxes were broadly consisted within global estimates and local nearby measurements.

Due to the complex topography, soil distributions, vegetation characteristics and microclimates with local moisture influence, plant water use is dynamic across small spatial scales (Berry et al., 2016). The slope difference results in varied exposure to (a) incoming solar radiation and (b) mean wind flow, which have an impact on the ET estimation and water partitioning but is captured by the spatially distributed model approach. Also, more exposed areas experience a faster heating during the day but are more efficient at cooling during the night. Therefore, modelled transpiration dynamics showed spatio-temporal differences (Figure 4c) according to the contrasting geomorphology of both hillslopes. The northern hillslope with lower slope gradient, more developed and deeper soils, higher vegetation density and higher LAI presented greater transpiration rates compared to the steeper southern slope (Figure 4b,c). Spatially, the difference in transpiration rates highlighted that during wet conditions and reduced transpiration, the difference between both hillslopes became less evident. Even though we presented simulated transpiration, our results are in accordance with findings reported by Aparecido et al. (2016) using in situ measurements from trees in a nearby tropical rainforest catchment (maximum values ~1.4 mm/day for wet and 0.6 mm/day for dry conditions). Future work will point at separating dew deposition from transpiration and rain interception (Gerlein-Safdi et al., 2018), which is hypothesized a key additional component influencing transpiration in humid tropical forests.

5.3 | What are the dominant controls on water ages?

Several recent studies showed the spatial and temporal non-stationary nature of water ages (Ala-aho et al., 2017; Hrachowitz et al., 2013; Piovano et al., 2019; Remondi et al., 2018), and assessed the influence of catchment characteristics on the modelled response (Dimitrova-Petrova, Geris, Wilkinson, Lilly, & Soulsby, 2019; Remondi et al., 2018). However, this study is novel in the use of a high temporal (hourly) and spatial (10 m grid) resolution for a detailed water age interpretation from a fully distributed landscape perspective. The simulated time series of water ages provided insights into the runoff generation processes and their controlling catchment characteristics.

Overall, the ranges of water ages simulated with STARR*tropics* matched the global estimates of age distributions recently presented by Sprenger et al. (2019). The transpiration flux age depends on species, their root distributions and uptake depth (Brinkmann et al., 2018; Sprenger et al., 2018) and in our case additionally on simplifying model assumptions of non-fractionating transpiration. Despite no simulated and observed evidence of evaporative fractionation in soil and streamwater, such assumptions can only be challenged by more soil, plant and atmosphere isotope data. Nonetheless, our young transpiration ages (deep and shallow) were comparable with the ages reported for vegetation (from hours to less than 1 year), due to the fact that tropical plant species tend to have large leaves with small boundary layer conductance (Perez & Feeley, 2018) accelerating fast water flow into the atmosphere. The youngest simulated transpiration was found on the hillslope with higher LAI and higher transpiration rates, while the oldest transpired water appeared in the riparian areas, again evidencing the dominant role of these landscape units as an important water source for ecohydrological processes (Snyder & Williams, 2000; Tetzlaff, Birkel, Dick, Geris, & Soulsby, 2014; van Huijgevoort et al., 2016a).

Additionally, tropical plant xylem water from understorey species and mature forests consistently uses water from topsoil layers (Goldsmith et al., 2012) instead of deeper groundwater because the root length density usually decreases rapidly with depth (Brantley et al., 2017) as empirically observed for several soil profiles at the study site. Clearly, uncertainties arise from the mixing assumptions implemented in the model (Hrachowitz et al., 2013) and a complete mixing is rather unrealistic (Good, Noone, & Bowen, 2015). However, partial mixing algorithms require additional model parameters that can only be justified with additional data on soil isotopes. With our limited observations, we therefore preferred to keep the number of calibrated parameters to a minimum in an attempt to avoid unnecessary model uncertainties.

Moreover, water ages from soils ranged from 1 to 5 months (Figures 5 and 6), which is younger but comparable with global references for bound and mobile soil water (Sprenger et al., 2019). Timbe et al. (2014) reported MTTs of soil water ranging from 2 to 9 weeks in a tropical montane rainforest catchment in the south of Ecuador. Despite being a valid catchment indicator, our approach considers the non-stationary nature of water ages. Groundwater ages (2–3.3 years) were in line with reported ages from other headwaters catchments elsewhere (Burns et al., 2003), but we did not find any evidence for deeper and older groundwater contributions to streamflow.

The stream water age cumulative distribution functions exhibited a young water dominance (Jasechko, Kirchner, Welker, & McDonnell, 2016), emphasizing the rapid rainfall-runoff and material transport dynamics of the catchment (Solano-Rivera et al., 2019). Overall, the stream water ages suggested dominance of active, frequent near-surface flow pathways (Solano-Rivera et al., 2019) in line with previous non-stationary water ages of less than 1 year in a similar humid tropical but mixed land use catchment in Costa Rica (Birkel et al., 2016). Simulated stream water ages varied seasonally depending on the wetness conditions (Harman, 2015). We clearly showed that stream water ages were younger in wetter conditions during the rainy season from May to December compared to drier periods from January to April (Birkel & Soulsby, 2016).

The hydrological connectivity that drives water displacement is highly variable in time and space (Jencso et al., 2009). Soil water within the catchment and spatially located on the northern hillslope and in riparian areas showed higher water ages and likely mixing with waters from different soil depths can increase the stream water age in drier conditions (Tetzlaff et al., 2009). Riparian zones in a northern upland catchment generally exhibited longer residence times than on the hillslopes (Soulsby et al., 2015) comparable to our findings. Therefore, young water from shallow soil horizons and mainly located at the foot slopes rapidly drain towards the channel network with little mixing, influencing the shorter stream water age in wetter conditions. Such findings from our tropical rainforest were consistent with other research in headwater catchments (Birkel, Soulsby, & Tetzlaff, 2012; Correa et al., 2017; Sánchez-Murillo et al., 2019; Tetzlaff et al., 2009; van Huijgevoort et al., 2016b). Despite limited average groundwater contribution to streamflow of only around 10% (Dehaspe et al., 2018), stream water ages significantly increased when shallow flow paths with younger ages were disconnected from the hydrological system of the catchment (Sprenger et al., 2019). Older water with constant isotope compositions is mainly located in the valley bottom without distinction between hillslopes.

Despite the experimental limitations of this study, our results provided useful insights into eco-hydrological processes related to landscape characteristics that control water age distributions in the quest for a more complete understanding of hydrologic functioning of tropical headwaters such as the San Lorencito catchment. The future of tropical eco-hydrology (Wright et al., 2018) depends on obtaining quality data to further challenge models such as STARR*tropics* and future work will aim at recollecting soil, xylem and atmospheric water vapour isotope compositions at our site.

6 | CONCLUSIONS

We developed an isotope-based transpiration mass balance and water age tracking for the STARR*tropics* model (Dehaspe et al., 2018) that allowed us to separate the evapotranspiration flux into its individual components for an eco-hydrologic assessment and evaluation of water ages in a pristine tropical rainforest catchment in northern Costa Rica. We found that:

1. Transpiration represented the dominant water flux to the atmosphere (65%) and varied spatially in relation to vegetation, soils and topography and temporally as a function of hydroclimatic conditions.
2. Overall, the system was dominated by younger water, ranging from 1 hr-transpiration to 3.3 years-old groundwater. The water ages increased during dry conditions.
3. Highest mean soil water ages were related to more developed soils and the water age of groundwater increased towards the bottom of the catchment.
4. Transpired water age was the youngest water flux when the plants uptake water from the shallowest soil horizon and approached soil water age when the water was uptaken from deeper soil horizons.

The stream water ages integrating all catchment processes showed a younger water system with little evidence for deeper and older groundwater. Despite the limitations of observed data (e.g., no available measurements of isotopes in water vapour, soil water and vegetation), to our knowledge, this is the first study in the tropics that quantitatively evaluated water age distributions in relation to landscape characteristics at such a high spatial and temporal resolution. This research demonstrated that the STARR*tropics* model consistently represented simple eco-hydrological processes in a non-stationary complex humid tropical catchment, with potential application elsewhere as a tool to inform land and water management to sustain ecosystem services.

ACKNOWLEDGEMENTS

The University of Costa Rica (project B8709) supported this project. We are grateful for support from the Ministry of Science and Technology of Costa Rica (MiCITT) under the B7507 grant, IsoNet and the University Centre for Advanced Studies (UCREA – B8276), the Leverhulme Trust through the ISOLAND project (RPG 2018 375), an IAEA CRP-22904 research contract, and the staff and students from the Global Change Observatory at the Department of Geography

(OACG). AC would like to acknowledge support by a UCR postdoctoral fellowship. All staff at the ReBAMB field station is thanked for continuous support. Finally, we thank the AE Paolo Benettin and three anonymous Reviewers for their valuable suggestions that helped improve earlier versions of this paper.

DATA AVAILABILITY STATEMENT

The data that support the findings of this research are available from the corresponding author upon request.

ORCID

Alicia Correa https://orcid.org/0000-0001-6127-2948
Christian Birkel https://orcid.org/0000-0002-6792-852X
Ana María Durán-Quesada https://orcid.org/0000-0003-0913-0154
Chris Soulsby https://orcid.org/0000-0001-6910-2118
Ricardo Sánchez-Murillo https://orcid.org/0000-0001-8721-8093

REFERENCES

Ala-aho, P., Tetzlaff, D., McNamara, J. P., Laudon, H., & Soulsby, C. (2017). Using isotopes to constrain water flux and age estimates in snow-influenced catchments using the STARR (spatially distributed tracer-aided rainfall–runoff) model. *Hydrology and Earth System Sciences*, *21*(10), 5089–5110. https://doi.org/10.5194/hess-21-5089-2017

Allen, R. G., Pereira, L. S., Raes, D., & Smith, M. (1998). Crop evapotranspiration—Guidelines for computing crop water requirements—FAO Irrigation and drainage paper 56. 15.

Allen, S. T., Kirchner, J. W., Braun, S., Siegwolf, R. T. W., & Goldsmith, G. R. (2019). Seasonal origins of soil water used by trees. *Hydrology and Earth System Sciences*, *23*(2), 1199–1210. https://doi.org/10.5194/hess-23-1199-2019

Amador, J. A. (2008). The intra-Americas sea low-level jet: Overview and future research. *Annals of the New York Academy of Sciences*, *1146*, 153–188. https://doi.org/10.1196/annals.1446.012, 2008.

Aparecido, L., Miller, G. R., Cahill, A. T., & Moore, G. W. (2016). Comparison of tree transpiration under wet and dry canopy conditions in a Costa Rican premontane tropical forest. *Hydrological Processes*, *30*(26), 5000–5011. https://doi.org/10.1002/hyp.10960

Aparecido, L., Miller, G. R., Cahill, A. T., & Moore, G. W. (2017). Leaf surface traits and water storage retention affect photosynthetic responses to leaf surface wetness among wet tropical forest and semi-arid savanna plants. *Tree Physiology*, *37*(10), 1285–1300. https://doi.org/10.1093/treephys/tpx092

Balzer, L., Schulz, K., Birkel, C., & Biester, H. (2020). Iron oxides control sorption and mobilisation of iodine in a tropical rainforest catchment. *SOIL Discussions*, 1–18. https://doi.org/10.5194/soil-2020-20

Berkelhammer, M., Noone, D. C., Wong, T. E., Burns, S. P., Knowles, J. F., Kaushik, A., … Williams, M. W. (2016). Convergent approaches to determine an ecosystem's transpiration fraction. *Global Biogeochemical Cycles*, *30*(6), 933–951. https://doi.org/10.1002/2016GB005392

Berry, Z. C., Gotsch, S. G., Holwerda, F., Muñoz-Villers, L. E., & Asbjornsen, H. (2016). Slope position influences vegetation-atmosphere interactions in a tropical montane cloud forest. *Agricultural and Forest Meteorology*, *221*, 207–218. https://doi.org/10.1016/j.agrformet.2016.02.012

Beven, K., & Westerberg, I. (2011). On red herrings and real herrings: disinformation and information in hydrological inference. *Hydrological Processes*, *25*, 1676–1680. https://doi.org/10.1002/hyp.7963, 2011.

Beven, K. J., & Kirkby, M. J. (1979). A physically based, variable contributing area model of basin hydrology / un modèle à base physique de zone d'appel variable de l'hydrologie du bassin versant. *Hydrological Sciences Bulletin*, *24*(1), 43–69. https://doi.org/10.1080/02626667909491834

Birkel, C., Geris, J., Molina, M. J., Mendez, C., Arce, R., Dick, J., … Soulsby, C. (2016). Hydroclimatic controls on non-stationary stream water ages in humid tropical catchments. *Journal of Hydrology*, *542*, 231–240. https://doi.org/10.1016/j.jhydrol.2016.09.006

Birkel, C., & Soulsby, C. (2015). Advancing tracer-aided rainfall–runoff modelling: A review of progress, problems and unrealised potential. *Hydrological Processes*, *29*(25), 5227–5240. https://doi.org/10.1002/hyp.10594

Birkel, C., & Soulsby, C. (2016). Linking tracers, water age and conceptual models to identify dominant runoff processes in a sparsely monitored humid tropical catchment: Linking tracers, water age and conceptual models in the humid tropics. *Hydrological Processes*, *30*, 4477–4493. https://doi.org/10.1002/hyp.10941

Birkel, C., Soulsby, C., & Tetzlaff, D. (2012). Modelling the impacts of land-cover change on streamflow dynamics of a tropical rainforest headwater catchment. *Hydrological Sciences Journal*, *57*(8), 1543–1561. http://agris.fao.org/agris-search/search.do?recordID=US201400188025

Birkel, C., Soulsby, C., & Tetzlaff, D. (2014). Developing a consistent process-based conceptualization of catchment functioning using measurements of internal state variables. *Water Resources Research*, *50*(4), 3481–3501. https://doi.org/10.1002/2013WR014925

Brantley, S. L., Eissenstat, D. M., Marshall, J. A., Godsey, S. E., Balogh-Brunstad, Z., Karwan, D. L., … Weathers, K. C. (2017). Reviews and syntheses: On the roles trees play in building and plumbing the critical zone. *Biogeosciences*, *14*(22), 5115–5142. https://doi.org/10.5194/bg-14-5115-2017

Brinkmann, N., Seeger, S., Weiler, M., Buchmann, N., Eugster, W., & Kahmen, A. (2018). Employing stable isotopes to determine the residence times of soil water and the temporal origin of water taken up by Fagus sylvatica and *Picea abies* in a temperate forest. *New Phytologist*, *219*(4), 1300–1313. https://doi.org/10.1111/nph.15255

Bruijnzeel, L. A., & Veneklaas, E. J. (1998). Climatic conditions and tropical montane Forest productivity: The fog has not lifted yet. *Ecology*, *79*(1), 3–9. https://doi.org/10.1890/0012-9658(1998)079[0003:CCATMF]2.0.CO;2

Burns, D. A., Plummer, L. N., McDonnell, J. J., Busenberg, E., Casile, G. C., Kendall, C., … Schlosser, P. (2003). The geochemical evolution of Riparian ground water in a forested Piedmont catchment. *Groundwater*, *41*(7), 913–925. https://doi.org/10.1111/j.1745-6584.2003.tb02434.x

Chakraborty, S., Belekar, A. R., Datye, A., & Sinha, N. (2018). Isotopic study of intraseasonal variations of plant transpiration: An alternative means to characterise the dry phases of monsoon. *Scientific Reports*, *8*(1), 8647. https://doi.org/10.1038/s41598-018-26965-6

Correa, A., Windhorst, D., Tetzlaff, D., Crespo, P., Célleri, R., Feyen, J., & Breuer, L. (2017). Temporal dynamics in dominant runoff sources and flow paths in the Andean Páramo. *Water Resources Research*, *53*(7), 5998–6017. https://doi.org/10.1002/2016WR020187

Darcy, H. (1856). *Les fontaines publiques de la ville de Dijon exposition et application des principes à suivre et des formules à employer dans les questions de distribution d'eau, ouvrage terminé par un appendice relatif aux fournitures d'eau de plusieurs villes au filtrage des eaux et à la fabrication des tuyaux de fonte, de plomb, de tole et de bitume*, Paris: V. Dalmont, Libraire des Corps imperiaux des ponts et chaussées et des mines.

Davies, J., Beven, K., Nyberg, L., & Rodhe, A. (2011). A discrete particle representation of hillslope hydrology: Hypothesis testing in reproducing a tracer experiment at Gårdsjön, Sweden. *Hydrological Processes*, *25*(23), 3602–3612. https://doi.org/10.1002/hyp.8085

Dehaspe, J., Birkel, C., Tetzlaff, D., Sánchez-Murillo, R., Durán-Quesada, A. M., & Soulsby, C. (2018). Spatially distributed tracer-aided modelling to explore water and isotope transport, storage and mixing in a pristine, humid tropical catchment. *Hydrological Processes*, *32*(21), 3206–3224. https://doi.org/10.1002/hyp.13258

Delavau, C. J., Stadnyk, T., & Holmes, T. (2017). Examining the impacts of precipitation isotope input ($\delta^{18}O_{ppt}$) on distributed, tracer-aided hydrological modelling. *Hydrology and Earth System Sciences*, *21*(5), 2595–2614. https://doi.org/10.5194/hess-21-2595-2017

Denyer, P., & Kussmaul, S. (2000). Geología de Costa Rica. Editorial Tecnológica de Costa Rica. http://editorial.tec.ac.cr/catalogo/geologia-de-costa-rica/

Dimitrova-Petrova, K., Geris, J., Wilkinson, M. E., Lilly, A., & Soulsby, C. (2019). Using isotopes to understand the evolution of water ages in disturbed mixed land-use catchments. *Hydrological Processes*, *34*, 972–990. https://doi.org/10.1002/hyp.13627

Dray, S., Legendre, P., & Blanchet, G. (2009). Packfor: Forward Selection with permutation (Canoco p.46) version 0.0-8 from R-Forge. https://rdrr.io/rforge/packfor/

Durán-Quesada, A. M., Gimeno, L., & Amador, J. (2017). Role of moisture transport for Central American precipitation. *Earth System Dynamics*, *8*(1), 147–161. https://doi.org/10.5194/esd-8-147-2017

Evaristo, J., Jasechko, S., & McDonnell, J. J. (2015). Global separation of plant transpiration from groundwater and streamflow. *Nature*, *525*(7567), 91–94. https://doi.org/10.1038/nature14983

Evaristo, J., Kim, M., van Haren, J., Pangle, L. A., Harman, C. J., Troch, P. A., & McDonnell, J. J. (2019). Characterizing the fluxes and age distribution of soil water, plant water, and deep percolation in a model tropical ecosystem. *Water Resources Research*, *55*(4), 3307–3327. https://doi.org/10.1029/2018WR023265

Fatichi, S., & Pappas, C. (2017). Constrained variability of modeled T:ET ratio across biomes. *Geophysical Research Letters*, *44*(13), 6795–6803. https://doi.org/10.1002/2017GL074041

Feeley, K. J., Joseph, S. W., Nur, M. S., Kassim, A. R., & Davies, S. J. (2007). Decelerating growth in tropical forest trees. *Ecology Letters*, *10*(6), 461–469. https://doi.org/10.1111/j.1461-0248.2007.01033.x

Ferretti, D. F., Pendall, E., Morgan, J. A., Nelson, J. A., LeCain, D., & Mosier, A. R. (2003). Partitioning evapotranspiration fluxes from a Colorado grassland using stable isotopes: Seasonal variations and ecosystem implications of elevated atmospheric CO2. *Plant and Soil*, *254*(2), 291–303. https://doi.org/10.1023/A:1025511618571

Gerlein-Safdi, C., Koohafkan, M. C., Chung, M., Rockwell, F. E., Thompson, S., & Caylor, K. K. (2018). Dew deposition suppresses transpiration and carbon uptake in leaves. *Agricultural and Forest Meteorology*, *259*, 305–316. https://doi.org/10.1016/j.agrformet.2018.05.015

Ghimire, C. P., Bruijnzeel, L. A., Lubczynski, M. W., Zwartendijk, B. W., Odongo, V. O., Ravelona, M., & van Meerveld, H. J. I. (2018). Transpiration and stomatal conductance in a young secondary tropical montane forest: Contrasts between native trees and invasive understorey shrubs. *Tree Physiology*, *38*(7), 1053–1070. https://doi.org/10.1093/treephys/tpy004

Gibson, J. J., Birks, S. J., & Edwards, T. W. D. (2008). Global prediction of δA and δ2H-δ18O evaporation slopes for lakes and soil water accounting for seasonality. *Global Biogeochemical Cycles*, *22*(2), GB2031. https://doi.org/10.1029/2007GB002997

Goldsmith, G. R., Muñoz-Villers, L. E., Holwerda, F., McDonnell, J. J., Asbjornsen, H., & Dawson, T. E. (2012). Stable isotopes reveal linkages among ecohydrological processes in a seasonally dry tropical montane cloud forest. *Ecohydrology*, *5*(6), 779–790. https://doi.org/10.1002/eco.268

Gonfiantini, R. (1986). Environmental isotopes in lake studies. In P. Fritz & J. C. Fontes (Eds.), *The terrestrial environment* (pp. 113–168). Amsterdam: Elsevier.

Gonfiantini, R., Wassenaar, L. I., Araguas-Araguas, L., & Aggarwal, P. K. (2018). A unified Craig-Gordon isotope model of stable hydrogen and oxygen isotope fractionation during fresh or saltwater evaporation. *Geochimica et Cosmochimica Acta*, *235*, 224–236.

Good, S. P., Noone, D., & Bowen, G. J. (2015). Hydrologic connectivity constrains partitioning of global terrestrial water fluxes. *Science*, *349*(6244), 175–177.

Gotsch, S. G., Asbjornsen, H., & Goldsmith, G. R. (2016). Plant carbon and water fluxes in tropical montane cloud forests. *Journal of Tropical Ecology*, *32*(5), 404–420. https://doi.org/10.1017/S0266467416000341

Grant, G. E., & Dietrich, W. E. (2017). The frontier beneath our feet. *Water Resources Research*, *53*(4), 2605–2609. https://doi.org/10.1002/2017WR020835

Gröning, M., Lutz, H. O., Roller-Lutz, Z., Kralik, M., Gourcy, L., & Pöltenstein, L. (2012). A simple rain collector preventing water re-evaporation dedicated for δ18O and δ2H analysis of cumulative precipitation samples. *Journal of Hydrology*, *448–449*, 195–200. https://doi.org/10.1016/j.jhydrol.2012.04.041

Gupta, H. V., Kling, H., Yilmaz, K. K., & Martinez, G. F. (2009). Decomposition of the mean squared error and NSE performance criteria: Implications for improving hydrological modelling. *Journal of Hydrology*, *377*(1–2), 80–91. https://doi.org/10.1016/j.jhydrol.2009.08.003

Harman, C. J. (2015). Time-variable transit time distributions and transport: Theory and application to storage-dependent transport of chloride in a watershed. *Water Resources Research*, *51*(1), 1–30. https://doi.org/10.1002/2014WR015707

Hidalgo, H. G., Amador, J. A., Alfaro, E. J., & Quesada, B. (2013). Hydrological climate change projections for Central America. *Journal of Hydrology*, *495*, 94–112. https://doi.org/10.1016/j.jhydrol.2013.05.004

Hoelscher, D., Koehler, L., van Dijk, A. I. J. M., & Bruijnzeel, L. A. (2004). The importance of epiphytes to total rainfall interception by a tropical montane rain forest in Costa Rica. *Journal of Hydrology*, *292*, 308–322. https://doi.org/10.1016/j.jhydrol.2004.01.015

Holdridge, L. R. (1967). *Life zone ecology*, San José, Costa Rica: Tropical Science Center.

Horita, J., & Wesolowski, D. J. (1994). Liquid-vapor fractionation of oxygen and hydrogen isotopes of water from the freezing to the critical temperature. *Geochimica et Cosmochimica Acta*, *58*(16), 3425–3437. https://doi.org/10.1016/0016-7037(94)90096-5

Hrachowitz, M., Savenije, H., Bogaard, T. A., Tetzlaff, D., & Soulsby, C. (2013). What can flux tracking teach us about water age distribution patterns and their temporal dynamics? *Hydrology and Earth System Sciences*, *17*(2), 533–564. https://doi.org/10.5194/hess-17-533-2013

Jasechko, S., Kirchner, J. W., Welker, J. M., & McDonnell, J. J. (2016). Substantial proportion of global streamflow less than three months old. *Nature Geoscience*, *9*(2), 126–129. https://doi.org/10.1038/ngeo2636

Jasechko, S., Sharp, Z. D., Gibson, J. J., Birks, S. J., Yi, Y., & Fawcett, P. J. (2013). Terrestrial water fluxes dominated by transpiration. *Nature*, *496*(7445), 347–350. https://doi.org/10.1038/nature11983

Jencso, K. G., McGlynn, B. L., Gooseff, M. N., Wondzell, S. M., Bencala, K. E., & Marshall, L. A. (2009). Hydrologic connectivity between landscapes and streams: Transferring reach- and plot-scale understanding to the catchment scale. *Water Resources Research*, *45*(4), W04428. https://doi.org/10.1029/2008WR007225

Karssenberg, D., Schmitz, O., Salamon, P., de Jong, K., & Bierkens, M. F. P. (2010). A software framework for construction of process-based stochastic spatio-temporal models and data assimilation. *Environmental Modelling & Software*, *25*(4), 489–502. https://doi.org/10.1016/j.envsoft.2009.10.004

Kirchner, J. W. (2016). Aggregation in environmental systems–Part 1: Seasonal tracer cycles quantify young water fractions, but not mean transit times, in spatially heterogeneous catchments. *Hydrology and Earth System Sciences*, *20*(1), 279–297. https://doi.org/10.5194/hess-20-279-2016

Knighton, J., Saia, S. M., Morris, C. K., Archiblad, J. A., & Walter, M. T. (2017). Ecohydrologic considerations for modeling of stable water isotopes in a small intermittent watershed. *Hydrological Processes*, *31*(13), 2438–2452. https://doi.org/10.1002/hyp.11194

Kuppel, S., Tetzlaff, D., Maneta, M. P., & Soulsby, C. (2018). What can we learn from multi-data calibration of a process-based ecohydrological model? *Environmental Modelling & Software*, *101*, 301–316. https://doi.org/10.1016/j.envsoft.2018.01.001

Magaña, V., Amador, J. A., & Medina, S. (1999). The midsummer drought over Mexico and Central America. *Journal of Climate*, *12*(6), 1577–1588. https://doi.org/10.1175/1520-0442(1999)012<1577:TMDOMA>2.0.CO;2

McDonnell, J. J., & Beven, K. (2014). Debates—The future of hydrological sciences: A (common) path forward? A call to action aimed at understanding velocities, celerities and residence time distributions of the headwater hydrograph. *Water Resources Research*, *50*(6), 5342–5350. https://doi.org/10.1002/2013WR015141

Meinzer, F. C., Goldstein, G., Holbrook, N. M., Jackson, P., & Cavelier, J. (1993). Stomatal and environmental control of transpiration in a lowland tropical forest tree. *Plant*, *Cell & Environment*, *16*(4), 429–436. https://doi.org/10.1111/j.1365-3040.1993.tb00889.x

Moore, G. W., Orozco, G., Aparecido, L. M. T., & Miller, G. R. (2018). Upscaling transpiration in diverse forests: Insights from a tropical premontane site. *Ecohydrology*, *11*(3), e1920. https://doi.org/10.1002/eco.1920

Munksgaard, N. C., Zwart, C., Kurita, N., Bass, A., Nott, J., & Bird, M. I. (2015). Stable isotope anatomy of tropical cyclone ITA, North-Eastern Australia, April 2014. *PLoS One*, *10*(3), e0119728. https://doi.org/10.1371/journal.pone.0119728

Nash, J. E., & Sutcliffe, J. V. (1970). River flow forecasting through conceptual models part I — A discussion of principles. *Journal of Hydrology*, *10*(3), 282–290. https://doi.org/10.1016/0022-1694(70)90255-6

Ochoa-Tocachi, B. F., Buytaert, W., De Bièvre, B., Célleri, R., Crespo, P., Villacís, M., … Arias, S. (2016). Impacts of land use on the hydrological response of tropical Andean catchments: Ochoa-Tocachi *et al*.: Land Use Impacts on Tropical Andean Hydrology. *Hydrological Processes*, *30*(22), 4074–4089. https://doi.org/10.1002/hyp.10980

Perez, T. M., & Feeley, K. J. (2018). Increasing humidity threatens tropical rainforests. *Frontiers in Ecology and Evolution*, *6*, 68. https://doi.org/10.3389/fevo.2018.00068

Picarro. (2010). ChemCorrectTM - Solving the Problem of Chemical Contaminants in H2 0 Stable Isotope Research. White Paper, 2–4.

Piovano, T. I., Tetzlaff, D., Carey, S. K., Shatilla, N. J., Smith, A., & Soulsby, C. (2019). Spatially distributed tracer-aided runoff modelling and dynamics of storage and water ages in a permafrost-influenced catchment. *Hydrology and Earth System Sciences*, *23*(6), 2507–2523. https://doi.org/10.5194/hess-23-2507-2019

Remondi, F., Kirchner, J. W., Burlando, P., & Fatichi, S. (2018). Water flux tracking with a distributed hydrological model to quantify controls on the spatio-temporal variability of transit time distributions. *Water Resources Research*, *54*(4), 3081–3099. https://doi.org/10.1002/2017WR021689

Rinaldo, A., Beven, K. J., Bertuzzo, E., Nicotina, L., Davies, J., Fiori, A., … Botter, G. (2011). Catchment travel time distributions and water flow in soils. *Water Resources Research*, *47*(7), 1–13. https://doi.org/10.1029/2011WR010478

Rutter, A. J., Kershaw, K. A., Robins, P. C., & Morton, A. J. (1971). A predictive model of rainfall interception in forests, 1. Derivation of the model from observations in a plantation of Corsican pine. *Agricultural Meteorology*, *9*, 367–384. https://doi.org/10.1016/0002-1571(71)90034-3

Rutter, A. J., Morton, A. J., & Robins, P. C. (1975). A predictive model of rainfall interception in forests. II. Generalization of the model and comparison with observations in some coniferous and hardwood stands. *Journal of Applied Ecology*, *12*(1), 367–380. https://doi.org/10.2307/2401739

Sáenz, F., & Durán-Quesada, A. M. (2015). A climatology of low level wind regimes over Central America using a weather type classification approach. *Frontiers in Earth Science*, *3*, 1–18. https://doi.org/10.3389/feart.2015.00015

Salazar, A. (2003). RESERVA BIOLOGICA ALBERTO ML. BRENES: Una excepción en Costa Rica. *InterSedes*, *5*(8), 2215–2458. https://revistas.ucr.ac.cr/index.php/intersedes/article/view/804

Sánchez-Murillo, R., Birkel, C., Welsh, K., Esquivel-Hernández, G., Corrales-Salazar, J., Boll, J., … Araguás-Araguás, L. J. (2016). Key drivers controlling stable isotope variations in daily precipitation of Costa Rica: Caribbean Sea versus eastern Pacific Ocean moisture sources. *Quaternary Science Reviews*, *131*, 250–261. https://doi.org/10.1016/j.quascirev.2015.08.028

Sánchez-Murillo, R., Romero-Esquivel, L. G., Jiménez-Antillón, J., Salas-Navarro, J., Corrales-Salazar, L., Álvarez-Carvajal, J., … Birkel, C. (2019). DOC transport and export in a dynamic tropical catchment. *Journal of Geophysical Research: Biogeosciences*, *124*(6), 1665–1679. https://doi.org/10.1029/2018JG004897

Schlesinger, W. H., & Jasechko, S. (2014). Transpiration in the global water cycle. *Agricultural and Forest Meteorology*, *189–190*, 115–117. https://doi.org/10.1016/j.agrformet.2014.01.011

Seibert, J., & Beven, K. J. (2009). Gauging the ungauged basin: How many discharge measurements are needed? *Hydrology and Earth System Sciences*, *13*(6), 883–892. https://doi.org/10.5194/hess-13-883-2009

Seibert, J., & Vis, M. J. P. (2012). Teaching hydrological modeling with a user-friendly catchment-runoff-model software package. *Hydrology and Earth System Sciences*, *16*(9), 3315–3325. https://doi.org/10.5194/hess-16-3315-2012

Seibert, J., & McDonnell, J. J. (2002). On the dialog between experimentalist and modeler in catchment hydrology: Use of soft data for multicriteria model calibration. *Water Resources Research*, *38*(11), 1241. https://doi.org/10.1029/2001WR000978

Smith, A. A., Tetzlaff, D., & Soulsby, C. (2018). Using StorAge selection functions to quantify ecohydrological controls on the time-variant age of evapotranspiration, soil water, and recharge. *Hydrology and Earth System Sciences Discussions*, 1–25. https://doi.org/10.5194/hess-2018-57

Snyder, K. A., & Williams, D. G. (2000). Water sources used by riparian trees varies among stream types on the San Pedro River, Arizona. *Agricultural and Forest Meteorology*, *105*(1/3), 227–240.

Solano-Rivera, V., Geris, J., Granados-Bolaños, S., Brenes-Cambronero, L., Artavia-Rodríguez, G., Sánchez-Murillo, R., & Birkel, C. (2019). Exploring extreme rainfall impacts on flow and turbidity dynamics in a steep, pristine and tropical volcanic catchment. *Catena*, *182*, 104118. https://doi.org/10.1016/j.catena.2019.104118

Soulsby, C., Birkel, C., Geris, J., Dick, J., Tunaley, C., & Tetzlaff, D. (2015). Stream water age distributions controlled by storage dynamics and nonlinear hydrologic connectivity: Modeling with high-resolution isotope data. *Water Resources Research*, *51*(9), 7759–7776. https://doi.org/10.1002/2015WR017888

Soulsby, C., Birkel, C., & Tetzlaff, D. (2016). Characterizing the age distribution of catchment evaporative losses. *Hydrological Processes*, *30*(8), 1308–1312. https://doi.org/10.1002/hyp.10751

Sprenger, M., Stumpp, C., Weiler, M., Aeschbach, W., Allen, S. T., Benettin, P., … Werner, C. (2019). The demographics of water: A review of water ages in the critical zone. *Reviews of Geophysics*, *57*(3), 800–834. https://doi.org/10.1029/2018RG000633

Sprenger, M., Tetzlaff, D., Buttle, J., Laudon, H., & Soulsby, C. (2018). Water ages in the critical zone of long-term experimental sites in northern latitudes. *Hydrology and Earth System Sciences*, *22*(7), 3965–3981. https://doi.org/10.5194/hess-22-3965-2018

Stadnyk, T. A., Delavau, C., Kouwen, N., & Edwards, T. W. D. (2013). Towards hydrological model calibration and validation: Simulation of stable water isotopes using the isoWATFLOOD model. *Hydrological Processes*, *27*(25), 3791–3810. https://doi.org/10.1002/hyp.9695

Stoy, P. C., El-Madany, T. S., Fisher, J. B., Gentine, P., Gerken, T., Good, S. P., … Wolf, S. (2019). Reviews and syntheses: Turning the challenges of partitioning ecosystem evaporation and transpiration into opportunities. *Biogeosciences*, *16*(19), 3747–3775. https://doi.org/10.5194/bg-16-3747-2019

Sutanto, S. J., Wenninger, J., Coenders-Gerrits, A. M. J., & Uhlenbrook, S. (2012). Partitioning of evaporation into transpiration, soil evaporation and interception: A comparison between isotope measurements and a HYDRUS-1D model. *Hydrology and Earth System Sciences*, *16*(8), 2605–2616. https://doi.org/10.5194/hess-16-2605-2012

Tetzlaff, D., Birkel, C., Dick, J., Geris, J., & Soulsby, C. (2014). Storage dynamics in hydropedological units control hillslope connectivity, runoff generation, and the evolution of catchment transit time distributions. *Water Resources Research*, *50*(2), 969–985. https://doi.org/10.1002/2013WR014147

Tetzlaff, D., Seibert, J., Mcguire, K. J., Burns, D. A., Dunn, S. M., & Soulsby, C. (2009). How does landscape structure influence catchment transit time across geomorphologic provinces ? *Hydrological Processes*, *23*, 945–953. https://doi.org/10.1002/hyp.7240

Timbe, E., Windhorst, D., Crespo, P., Frede, H.-G., Feyen, J., & Breuer, L. (2014). Understanding uncertainties when inferring mean transit times of water trough tracer-based lumped-parameter models in Andean tropical montane cloud forest catchments. *Hydrology and Earth System Sciences*, *18*(4), 1503–1523. https://doi.org/10.5194/hess-18-1503-2014

van Huijgevoort, M. H. J., Tetzlaff, D., Sutanudjaja, E. H., & Soulsby, C. (2016a). Using high resolution tracer data to constrain water storage, flux and age estimates in a spatially distributed rainfall-runoff model. *Hydrological Processes*, *30*(25), 4761–4778. https://doi.org/10.1002/hyp.10902

van Huijgevoort, M. H. J., Tetzlaff, D., Sutanudjaja, E. H., & Soulsby, C. (2016b). Visualization of spatial patterns of connectivity and runoff ages derived from a tracer-aided model. *Hydrological Processes*, *30*(25), 4893–4895. https://doi.org/10.1002/hyp.10961

van Meerveld, H. J. (. I.)., Zhang, J., Tripoli, R., & Bruijnzeel, L. A. (2019). Effects of reforestation of a degraded Imperata grassland on dominant flow pathways and streamflow responses in Leyte, The Philippines. *Water Resources Research*, *55*(5), 4128–4148. https://doi.org/10.1029/2018WR023896

Willmott, C. J., & Matsuura, K. (2005). Advantages of the mean absolute error (MAE) over the root mean square error (RMSE) in assessing average model performance. *Climate Research*, *30*(1), 79–82. https://doi.org/10.3354/cr030079

Wohl, E., Barros, A., Brunsell, N., Chappell, N. A., Coe, M., Giambelluca, T., … Ogden, F. (2012). The hydrology of the humid tropics. *Nature Climate Change*, *2*(9), 655–662. https://doi.org/10.1038/nclimate1556

Wright, C., Kagawa-Viviani, A., Gerlein-Safdi, C., Mosquera, G. M., Poca, M., Tseng, H., & Chun, K. P. (2018). Advancing ecohydrology in the changing tropics: Perspectives from early career scientists. *Ecohydrology*, *11*(3), e1918. https://doi.org/10.1002/eco.1918

Zheng, G., & Moskal, L. M. (2009). Retrieving leaf area index (LAI) using remote sensing: Theories, methods and sensors. *Sensors*, *9*, 2719–2745. https://doi.org/10.3390/s90402719

How to cite this article: Correa A, Birkel C, Gutierrez J, et al. Modelling non-stationary water ages in a tropical rainforest: A preliminary spatially distributed assessment. *Hydrological Processes*. 2020;1–18. https://doi.org/10.1002/hyp.13925